EXPERIMENTAL MEASUREMENTS OF THE MEAN FLOW FIELD IN WIDE-ANGLED DIFFUSERS: A DATA BANK CONTRIBUTION

K. Kibicho[1] and A. T. Sayers[2]
[1]Department of Mechanical Engineering, Jomo Kenyatta University of Agriculture and Technology, Nairobi, Kenya
[2]Department of Mechanical Engineering, University of Cape Town, Rondebosch, South Africa
E-mail: kkibicho@eng.jkuat.ac.ke

ABSTRACT

Due to adverse pressure gradient along the diverging walls of wide-angled diffusers, the attached flow separates from one wall and remains attached permanently to the other wall in a process called stalling. Stalled diffusers render the whole fluid flow system, in which they are part of, very inefficient. There is then an engineering need to try to understand the whole process of diffuser stall if any meaningful attempts to improve on diffuser efficiency are to be made. In this regard, this paper provides a data bank contribution for the mean flow-field in wide-angled diffusers where the complete velocity and static pressure fields, and pressure recovery data for diffusers in the fully stalled flow regime are experimentally measured. The measurements were carried out at Reynolds numbers between 1.07×10^5 and 2.14×10^5 based on inlet hydraulic diameter and centerline velocity for diffusers whose divergence angles were between 30° and 50°. Variation of Reynolds number did not significantly affect the velocity and static pressure profiles. The wall static pressure recovery was found to be more sensitive to changes in the Reynolds number. By increasing the velocity from 10 m/s to 20 m/s, the wall static pressure recovery increased by 8.31%. However, as the divergence angle was increased, a similar increase in the Reynolds number resulted in a higher percentage increase in pressure recovery. Experimental results showed that regardless of the wall to which the flow was attached, both the velocity and pressure fields were replicated with discrepancies below 2%. Finally, by using the experimental data, a method to predict the distance along the wall where flow reversal first occurs (point of stall), is proposed.

Key words: Two-dimensional, wide-angled, diffuser, stall, separated flows, subsonic flows, diffuser flow regimes

1.0 INTRODUCTION

In many engineering applications, diffusers are used to convert kinetic energy into pressure energy. The importance of the diffuser as a single, useful, fluid-mechanical element in wind tunnels and turbo-machinery has been widely known. Understanding of diffuser flows, therefore, is of paramount importance to the design of fluid-flow systems. In the last few decades, a lot of experimental and computational research has been devoted to this subject. Unfortunately, even turbulent flows in two-dimensional diffusers are extremely complicated and our understanding of the details of energy transfer and dissipative losses inside a diffuser is still incomplete.

In order to meet some design constraints such as the overall size of a fluid-flow system, wide-angled diffusers with severe flow separation and poor efficiency, are often tolerated. The flow separation is caused mainly by the adverse pressure gradient along the walls of the diffuser, causing a back-flow, in a process known as 'stalling'. The back-flow behaviour of stalled diffusers is uniquely related to the diffuser geometry, as described in the flow regime chart of Fox and Kline (1962).

The convention commonly used for two-dimensional diffuser flows is given in Figure 1.

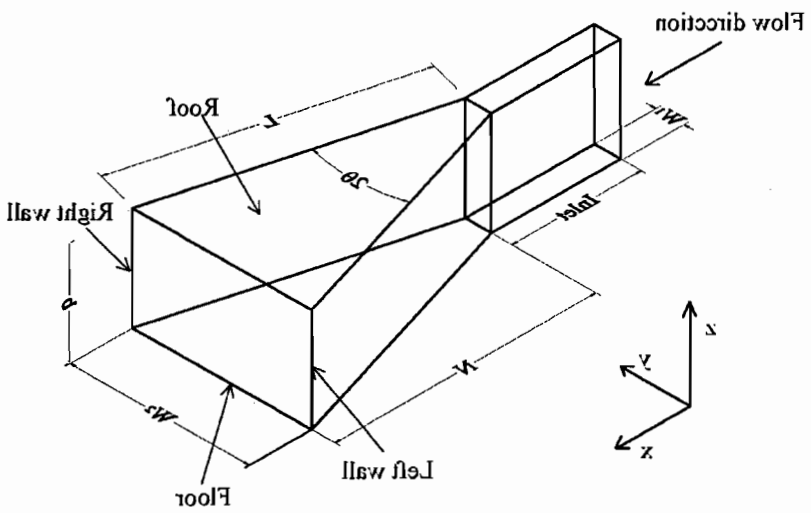

Figure 1: Two-dimensional diffuser geometry and the frame of reference

The relationship between diffuser geometry and performance is mainly covered by Reneau *et al.* (1967), Kline *et al.* (1959), and Sagi and Johnston (1967), among others. They concluded that the optimum effectiveness is achieved when the total

divergence angle of the diffuser is approximately 7° and the ratio $\frac{N}{W_1}$ not exceeding 25. They further reported that at high divergence angles, the area ratio became less significant as a variable for determining pressure recovery. Even though their work did not address the flow-structure within the diffusers and instead covered only the pressure recovery between the inlet and the outlet of the diffusers, the work of Reneau *et al.* (1967) is widely used in the design and mapping of two-dimensional diffusers.

The stalling phenomena in diffusers can be related to the rate of boundary layer growth in the inlet duct and within the diffuser. McMillan and Johnston (1973); Norbury (1959), and Johnston and Powars (1969) have argued that a uniform velocity profile carries the minimum momentum flux possible at a given flow rate, so transformation of a distorted profile to a more uniform one, even in a constant area duct, can result in an increase in static pressure (a process that occurs in diffuser tail pipes). However, uniform flow at the inlet of the diffuser is not always achieved in practice, since various upstream flow conditions like obstructions due to blades, struts, etc., may shed wakes. In any case, it is known that the introduction of the wide-angled diffuser causes severe non-uniformity in the upstream inlet channel. Based on this understanding therefore, the inlet core-flow velocity profile distortions can cause a significant change in the pressure-recovery performance and, by implication, the flow regimes.

Many researchers, among them, Reneau *et al.* (1967), and Sagi and Johnston (1967) have shown that at low Mach numbers, performance is quite insensitive to Reynolds number. Recently, Kibicho *et al.* (2001), and Kibicho and Sayers (2005) in fact confirmed this insensitivity and demonstrated that the velocity field within the wide-angled diffuser is little influenced by Reynolds number. Most of this experimental work was carried out at inlet Mach numbers below 0.2. Runstadler and Dean (1969) have investigated the effect of varying the diffuser inlet Mach number on both the flow regimes and the performance. Variation of Mach number at low flow Mach numbers marginally influenced the performance, while in supersonic flow regimes, there was little gain in performance as the Mach number was raised.

If the basic mechanisms that control diffuser performance can be understood, then, this will lead to the design of systems which employ techniques that utilise these mechanisms in improving the efficiency of fluid machines. Once the separation of the flow from the walls in adverse pressure gradients is prevented by any method, then, that method can be applied to design an efficient diffuser with a large divergence angle and a shorter length. Hoffmann (1981) has argued that if such a method can enhance the transfer of free stream turbulent energy to the diffuser walls, then this transfer of energy will decrease the distortion of the velocity profiles within the diffuser and delay the onset of separation.

2.0 EXPERIMENTAL APPARATUS AND INSTRUMENT

The experimental apparatus is shown in Figure 2. Air was delivered by a radial flow fan into a 1.9 m long, rectangular-circular transition duct, which was connected to a 600 mm inner diameter, 3.7 m long circular duct. A 1 m long circular-rectangular transition duct transferred the air to a 400 mm x 100 mm x 1 m long straight inlet duct before its entry into the diffuser proper. After flowing through the diffuser, the air was discharged back into the atmosphere.

All the plates for the straight inlet section and diffuser were machined from 10 mm thick transparent thermoplastic resin (Perspex). Details of the complete design of the flow facility, instrumentation and uncertainty analysis can be found in Kibicho (2006).

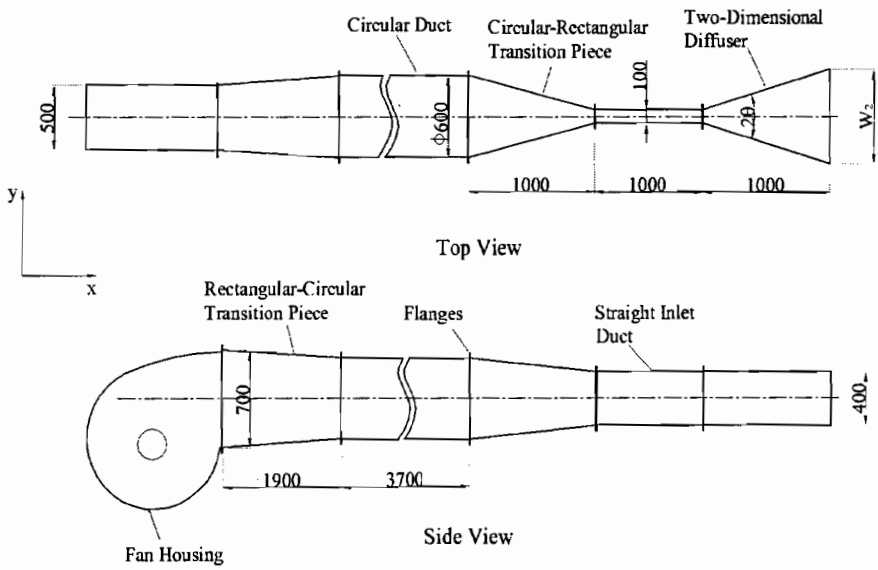

Figure 2: Experimental apparatus

Due to the manufacturing difficulties of drilling static pressure holes at the exact diffuser entry, a set of eight holes of 1.8 mm diameter were drilled at a location 2 mm upstream of the diffuser entry. The entry static pressure was averaged by connecting the eight static tubes to a common ring tube. The output of the common ring tube was the inlet static pressure, P_1.

The roof of the diffuser was constructed from six, 150 mm wide strips and two strips of widths 15 mm and 85 mm installed as the first and last strip at the entry and exit of the diffuser respectively. A 2 m long by 150 mm wide Perspex probing strip was used to move a 3-tube yaw meter in the y direction for measuring the velocity profiles across the diffuser test section. All the 150 mm wide roof strips were removed in turn and replaced with the probing strip.

The pressure recovery coefficient C_{pr} was evaluated according to the definition given in Equation 1.

$$C_p = \frac{P_x - P_1}{\frac{1}{2}\rho U_1^2} \quad \text{.....(1)}$$

where P_x is the pressure measured along the walls of the diffuser.

Streamwise velocity profiles were measured using a 3-tube yaw meter. The probe was calibrated against a hot-wire anemometer in a low-turbulence intensity (0.4% turbulence intensity) wind tunnel flow field. Non-dimensional calibration parameters were calculated in terms of pressures and resultant flow velocity, q, similar to those specified by Yajnik and Gupta (1973), and Rhagava *et al.*(1979) and given in Equations 2 and 3.

$$f(\psi) = \frac{P_l - P_r}{P_c - P_m} \quad \text{.....(2)}$$

$$Q_p = \frac{P_c - P_m}{\frac{1}{2}\rho q^2} \quad \text{.....(3)}$$

Where P_l and P_r are the pressures sensed by the off-centre tubes, $P_m = (P_l + P_r)/2$, is the mean pressure for the off-centre pressures, and P_c is the pressure measured by the central tube.

The reference probe null-position was selected as the direction of the centerline of the probe tip in line with the main flow direction when the pressures recorded from the off-centre tubes were equal to each other. At this reference direction, $\psi = 0°$. The pressure measured at the central tube of the probe at this position was the total (stagnation) pressure of the flow, P_t. These functions can be established directly and are known to be independent of Reynolds number. Thus, once established at one Reynolds number, they can be applied to a range of Reynolds numbers. Calibration of the probe was done at 15 m/s. Calibration charts of $f(\psi)$ and Q_p against ψ were therefore generated.

By using Eq. 2 to get $f(\psi)$, the flow angle, ψ was established at every measurement point from the charts. Thus, knowing ψ, Q_p was also read off the charts and Equation

3 used to evaluate the flow velocity, q. The velocity components u and v with respect to the x and y directions of the pressure probe, respectively, were then calculated according to Equation 4.

$$u = q\cos\psi$$
$$v = q\sin\psi \quad \text{.....(4)}$$

Results obtained by use of these equations were tested at several locations within the diffuser test section against the null-reading technique. The average error in measuring the flow angle was 0.81°. The rms error in velocity measurement was 1.37%.

3.0 RESULTS AND DISCUSSION

3.1 Tunnel Qualification

3.1.1 Inlet Channel Flow

Uniformity of inlet flow affects the diffuser performance as discussed by Wolf and Johnston (1969). In this respect, the inlet axial velocity profiles were measured, first without the diffuser and then repeated with the diffuser connected to the inlet duct. A measure of the non-uniformity of the flow, γ, was evaluated as the overall discrepancy of axial velocities u_i, measured at corresponding points to the right and left of the x-axis. A summary of the non-uniformities for all the diffusers with flow at different Reynolds numbers is given in Table 1.

Table 1: Non-uniformity, γ (%), of inlet flow with diffuser

Re×10^5	Re=1.08	Re=1.63	Re=2.18
30°	4.17	4.41	4.92
40°	4.21	4.42	4.77
50°	4.23	4.55	5.03

This non-uniformity of the flow caused the corresponding static pressures on the opposite side walls at the inlet to be different. This situation presented a problem in the interpretation of reference inlet conditions both for the velocity and static pressure data, since each flow condition produced different profiles. Consequently, it was found necessary to reference the inlet flow conditions to a location where the flow was reasonably uniform. Such a point was found to be at an arbitrarily chosen upstream location of $\frac{x}{W_1}$ = "2.35. At this inlet reference location, the axial velocity profiles were again measured, with and without the diffuser. The highest non-uniformity of the axial velocity profiles measured in both the y and z directions at the reference diffuser location was 0.23% for the 50° diffuser.

It still remains unclear why stalling in the two-dimensional fully stalled regime in diffusers occurs on a particular wall. Great care was taken to manufacture highly symmetrical diffusers. Tests to rule out the possibility of a bias towards the flow attaching to a particular wall whenever the fan was switched on were carried out. In this regard, for all diffusers and before any measurements were taken, a start-stop check was done whereby the fan was started, the wall to which the flow was attached noted, the fan switched off and started again and the process repeated. These tests were done at an inlet duct velocity of 15 m/s. An intermittency parameter γ_s, was then defined as a ratio of the number of times the flow remained attached to a given wall to the total number of start-stop cycles. γ_s was measured to have a maximum value of 0.60 in favor of the left hand wall for the 50° diffuser.

It was however possible to force the flow to attach to the other wall by partially blocking the flow at the inlet with a piece of Perspex, and directing it to the desired wall where the data acquisition system was positioned. Once 'switched' to the other side, the flow remained attached to that wall.

3.1.2 Reproducibility and Replication

Flows in wide-angled diffusers are inherently unsteady. In order to reduce the effect of the unsteadiness in the experimental results, the pressure transducer differential voltages were averaged over long durations. The optimal averaging duration was achieved by setting it at a given value and then measuring the velocities and static pressures at a few selected data points while holding the inlet velocity constant. The averaging period was then varied and the measurements at the same data points repeated. Thus, the optimal averaging duration corresponded to the period beyond which the velocity and static pressure readings ceased changing with change in averaging period. This optimal averaging time was kept constant for the rest of the measurements and it was only then that the repeatability tests to determine the overall experimental uncertainties were performed. Due to the large number of data points obtained especially when measuring the velocity profiles, it was found adequate to take readings at each point three times and then average their discrepancies for all the data points. In any case, the statement of overall uncertainties is all that is required. Figures 4 and 5 show typical reproducibility results obtained for the wall static pressure recovery and velocity field, respectively for a 30° diffuser. The reproducibility tests were however performed for all the other diffusers whose results are summarised in Table 2. Even though the reproducibility seems to worsen as both Reynolds number and divergence angles increased, the maximum discrepancy at 1.88% indicate fairly reproducible experiments of these physically complex flows.

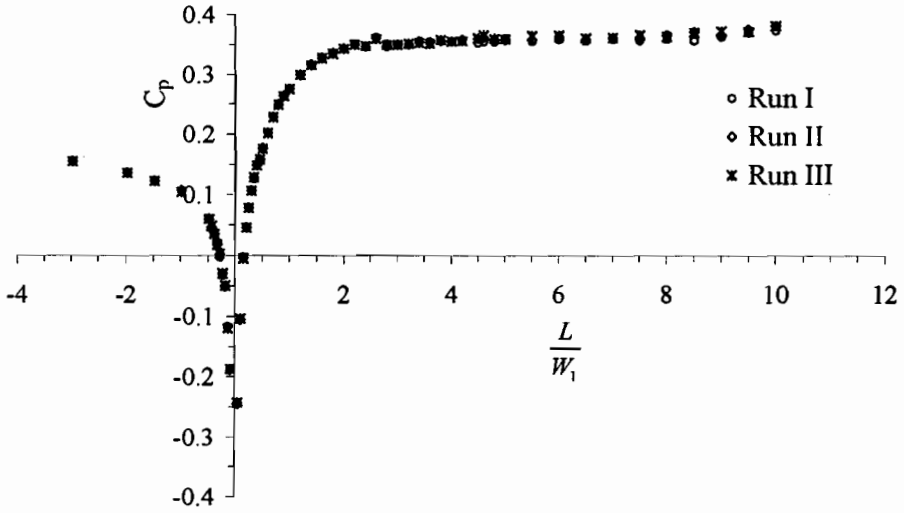

Figure 4: Reproducibility of C_p for the 30° diffuser

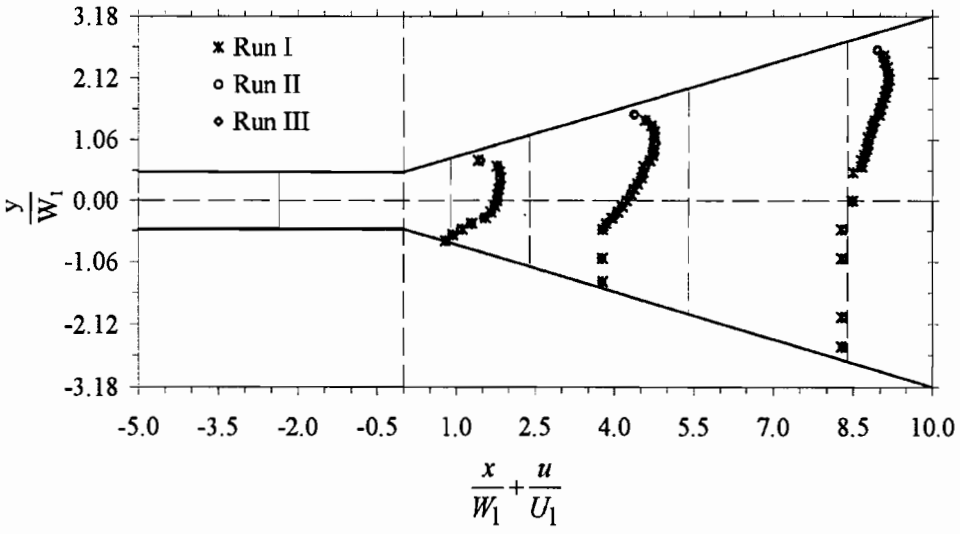

Figure 5: Reproducibility of velocity profiles for the 30° diffuser

As has already been observed, the wall to which the flow attached was quite random. However, since the data acquisition system was placed on the left side of the diffuser, the flow was always manually 'switched' to the left wall in instances when it attached to the right wall. With this in mind, it was important to confirm that both the pressure and velocity fields were independent of the wall to which flow was attached. To verify this requirement, the flow field was measured with the flow firstly attached to the left wall and secondly with the flow attached to the right wall, as can be seen from Figure 6. For ease of comparison, results of Figure 6, when the flow was attached to the right wall were reflected about the x-axis shown in Figure 7, leading to the choice of the term 'mirror replication' to describe the tests.

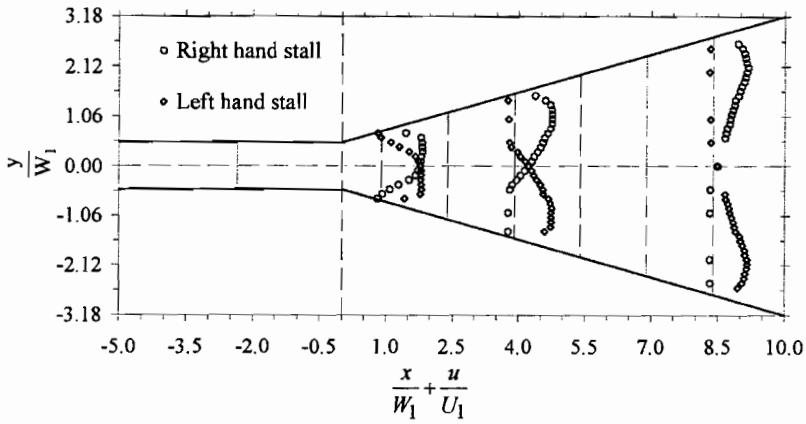

Figure 6: Replication of velocity profiles for the 30 ° diffuser

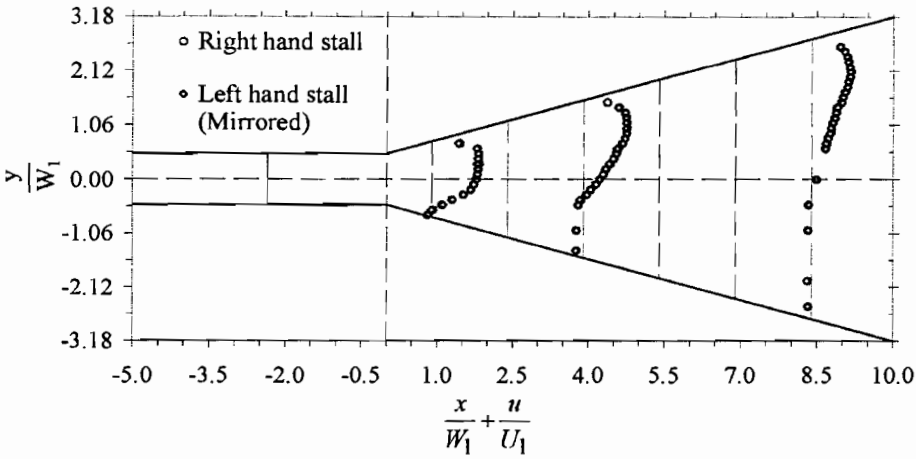

Figure 7: Mirror replication of velocity profiles for the 30 ° diffuser

Lastly, static pressures were measured on the wall to which the flow was attached (unstalled wall). Pressure recovery data for corresponding static pressure holes on the two walls is shown in Figure 8. These replication tests were performed for all the angles at the different Reynolds numbers and a summary of these results are given in Table 2.

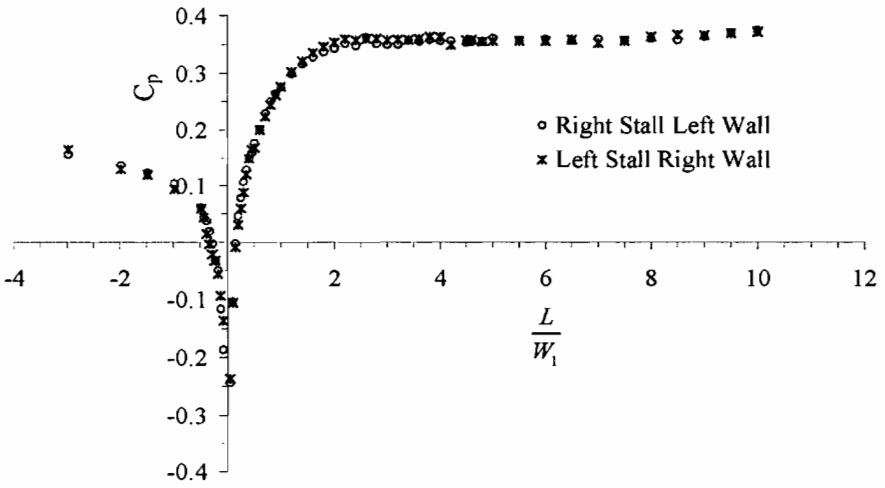

Figure 8: Replication of C_p for the 30° diffuser

Table 2. Reproducibility and replication of diffuser flows

	2θ	Reproducibility discrepancy, % Re×10⁵			Replication discrepancy, discrepancy, % Re×10⁵		
		1.08	1.63	2.18	1.08	1.63	2.18
C_{pr}	30°	1.42	1.57	1.63	1.77	1.85	1.97
	40°	1.53	1.61	1.70	1.91	1.97	2.01
	50°	1.66	1.72	1.88	1.93	1.99	2.13
	30°	0.32	0.36	0.37	0.52	0.55	0.57
	40°	0.34	0.33	0.39	0.53	0.56	0.58
	50°	0.36	0.37	0.34	0.56	0.58	0.59

The static pressure field showed more sensitivity to replication than the velocity profiles. The replication discrepancies for the static pressure field worsened as the flow velocity and divergence angle were increased. However, since the replication discrepancies are of the same order of magnitude as the reproducibility, they can be viewed to be a result of the flow unsteadiness and the small imperfections in the diffuser symmetry. The replication discrepancy of the velocity profiles was below 0.6% in all cases.

3.1.3 Reynolds Number Dependence

Although it is reported in the literature that variation of Reynolds number does not influence the pressure recovery data, the indications obtained while performing the reproducibility and replication tests, was that Reynolds number indeed has a significant influence on the flow field. It was therefore decided to perform tests to evaluate the influence of Reynolds number on both the static pressure and velocity fields. The inlet velocity was set at 10 m/s, 15 m/s and 20 m/s corresponding to Reynolds numbers 1.08×10^5, 1.63×10^5, 2.18×10^5, respectively. Preliminary tests showed that at velocities higher than 20 m/s, undesirable vibration of the diffusers was produced. Figures 9 and 10 show the influence of the Reynolds number on the wall static pressure recovery and velocity profiles respectively.

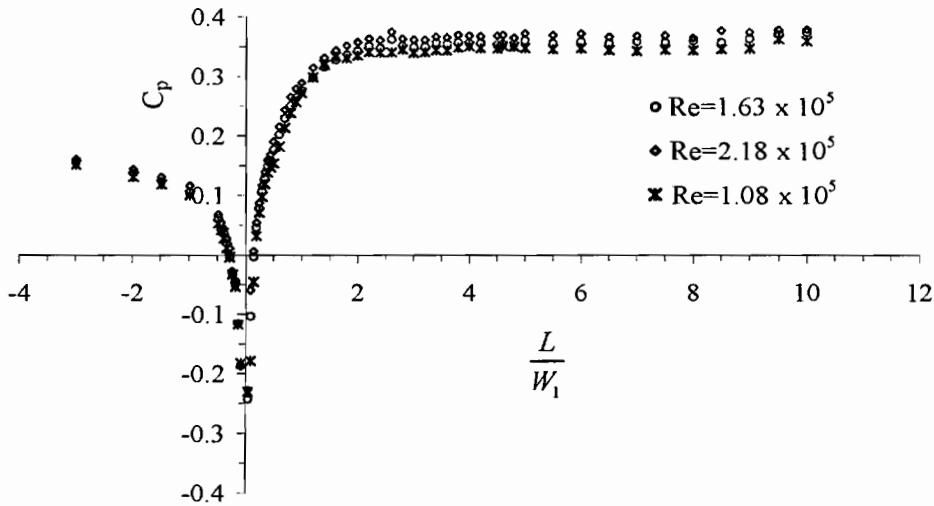

Figure 9: Influence of Re on C_p for the 30° diffuser

The sensitivity of C_p values to Reynolds number changes near the diffuser entry can be attributed to the three dimensionality nature of the flow expected in this region and to the fact that it is in this region that the highest adverse pressure gradients are experienced, rendering the flow here very unstable. Attempts to use the yaw meter to measure the velocity profiles in this region resulted in data whose reproducibility was above 15%. However, velocity profiles measured at the first strip (located 90 mm downstream of the diffuser inlet), indicated very little influence (of the order of 1%) on the profiles due to Reynolds numbers, as can be seen from Figure 10.

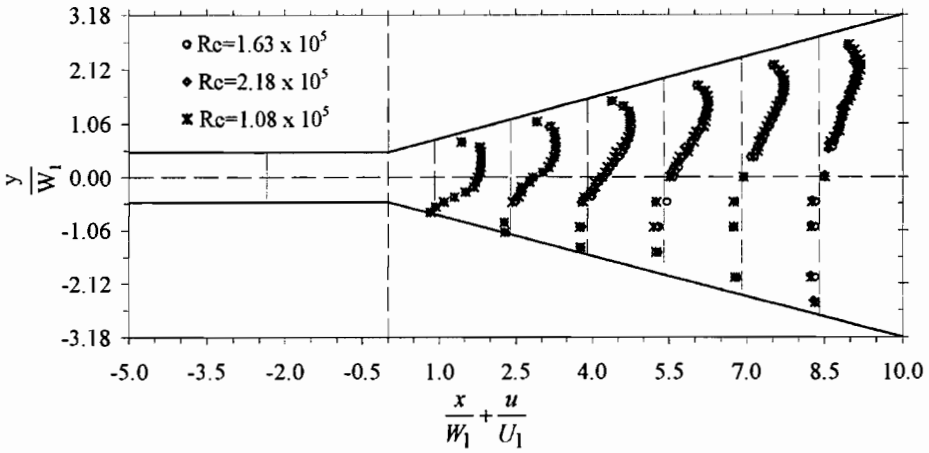

Figure 10: Influence of Re on velocity profiles for the 30 ° diffuser

Results show that by changing the velocity from 10 m/s to 20 m/s, the static pressure recovery increased by 8.31%, 10.15%, and 9.35% for 30°, 40° and 50° diffusers, respectively. A similar increase in Reynolds number for the velocity profiles showed that the increase of the normalised velocities was 1.37%, 1.57%, and 1.60% for 30°, 40° and 50° diffusers, respectively. Evidently, the static pressure was influenced by the Reynolds number at values that are outside the overall experimental uncertainties of about 2% in this study.

It might be of interest in future to carry out a study that can relate Reynolds number to diffuser geometry. Results from the limited number of flow cases in this study cannot be considered adequate to provide a reasonable correlation. Bearing this in mind and in order to focus on the primary objectives of this research, it was decided that from this point onwards, the Reynolds number be held constant at 1.63 $\times 10^5$ corresponding to an inlet duct velocity of 15 m/s.

3.1.4 Two-Dimensionality

The primary assumption made in this study is that the flow is two-dimensional. In fact, it is only due to this assumption that the three-tube yaw meter was used to measure the velocity vectors. All diffusers studied in this research had the roof and the floor walls running parallel to each other. It was rational to assume that the boundary layer growth rates from the floor and roof walls were the same and merged at the mid-plane. Therefore, measuring the flow in the mid-plane was adequately representative of a two-dimensional flow.

Traditionally, proof of two-dimensionality of a flow is carried out by measuring axial velocity profiles at two different planes, one below the mid-plane, and another above the mid-plane. Thus, for a given location within the diffuser, axial velocity profiles were measured in three planes, namely; upper, mid and lower planes. The upper and lower planes were both at a 100 mm distance from the roof and floor of the diffuser respectively. For all diffusers in this study, the two-dimensionality of the flow was verified using this procedure, with the velocity profiles being measured at three locations downstream of the diffuser inlet located at $\frac{x}{W_1} = 0.9, 3.9$ and 8.4. Typical results of such measurements are shown in Figure 11.

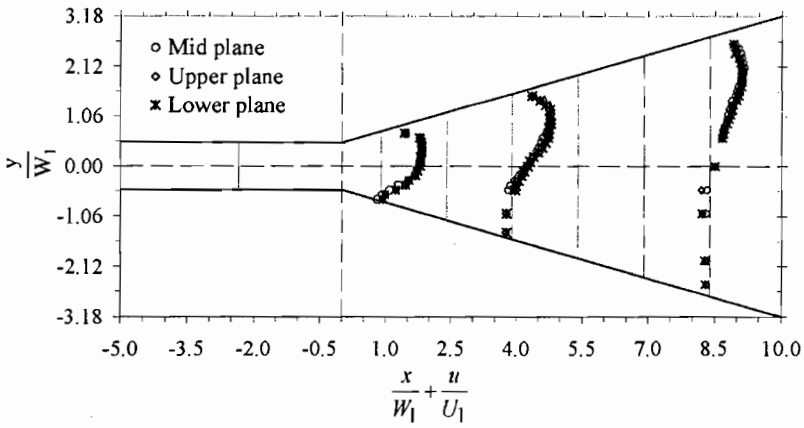

Figure 11: Two-dimensionality test for 30 ° diffuser

The velocity profiles in the upper and lower planes, for symmetrical boundary layer growth rates between roof and floor walls, must be the same. With the mid-plane held as the datum, the overall deviations from this plane for the lower and the upper planes are shown in Figure 12. The largest difference in these deviations between the upper and lower planes in Figure 12 was 0.3%, meaning that the two-dimensionality was well within the uncertainties of the experimental data in this study. However, the lower plane consistently gave higher discrepancies, in line with what Kline (1959) observed about the stall starting at a localised position on the lower corners of the diffuser before spreading to the rest of the diffuser.

Flow visualisation using woolen tufts was performed in order to observe the steadiness and two-dimensionality of the flow. The woolen tufts were attached to the sidewalls of the diffuser at several locations. Apart from the tufts that were next to the roof and floor, and which displayed slight fluctuations of movement, all the other tufts faced the downstream direction steadily and ran almost parallel to each other.

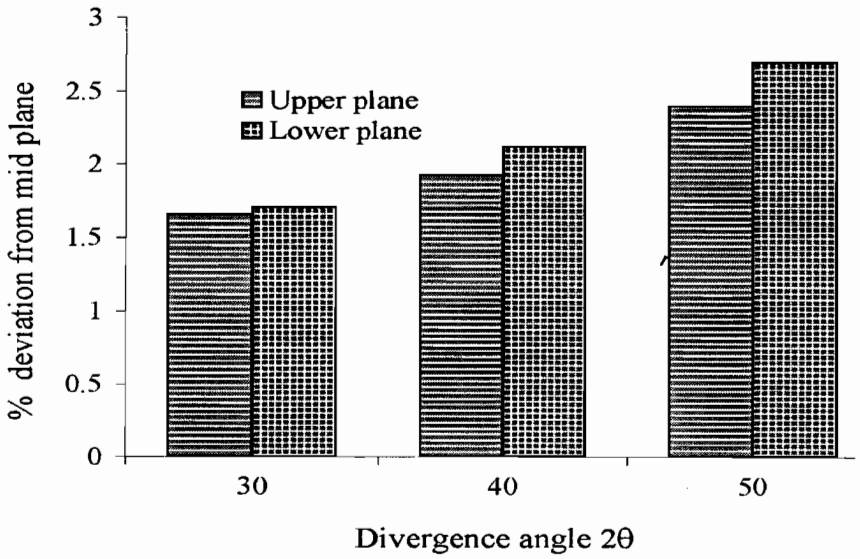

Figure 12: Discrepancies in the velocity profiles between planes

Further flow visualisation was carried out using thin tailor's thread. Long pieces of the thread were passed through corresponding static pressure holes across the width of the diffuser at several locations in the flow-field. On each of these threads, short pieces of thread about 20 mm long were tied at several points. Lastly, pieces of the tailor's thread were passed through each wall static pressure hole. Following, this treatment, the flow visualisation results shown in Figure 15, and to be discussed later, were obtained. On the unstalled wall near the diffuser inlet of the 50° diffuser, a separation bubble consistent with the notation of figure 15 was observed. This bubble was not present in the flow visualisation results of the 30° and 40° diffusers.

3.1.5 Data Bank Contribution

In the interest of clarity while discussing the experimental results, only representative cases of extensive experimental data have been presented. However, the same rigorous checks and experimental procedures, as already discussed, were performed for all flow cases. These results are presented in the appendix as a data bank contribution.

The results presented in the data bank include, the axial velocity profiles, $\frac{u}{U_1}$ and the wall static pressure recovery C_{pr}.

Comparison of the wall static pressure recovery data with data of previous researchers and some numerical work of Kibicho (2006) is shown in Figure 13.

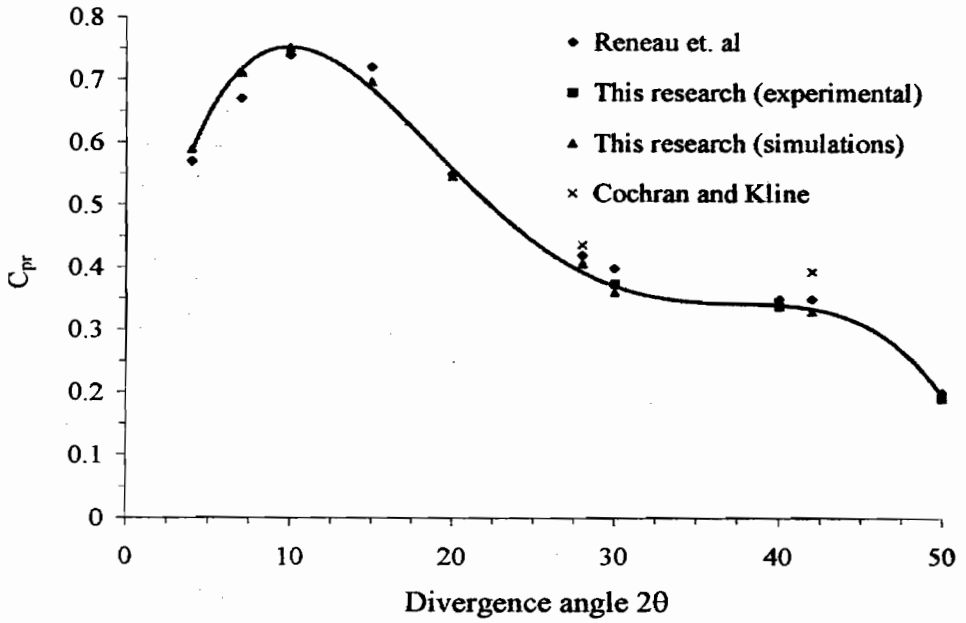

Figure 13: Comparison of C_{pr} data with previous data

3.1.6 Prediction of the Effective Flow Geometry

In wide-angled diffuser flows, the magnitude of the velocities in the stalled region is much lower than those in the unstalled region. From one-dimensional flow theory considerations, higher diffuser exit effective areas correspond to higher pressure recoveries. Thus, for prediction of the pressure recovery, the effective flow area, especially at the exit, is critical. The velocity profiles presented so far suggest the existence of an imaginary streamline that defines the transition between regions of stalled and unstalled flow. This streamline corresponds to the imaginary line of all the points where $u = 0$, measured while probing the velocities between the left and right walls of the diffusers as described below. The distances of all the six roof strips from the diffuser entry point in the x direction were known, and hence the width of each strip W_x, was evaluated according to Equation 5. The calculated width W_x was then used to normalise distances measured in the y direction about the x-axis for each strip. A normalised length scale ξ, was then defined and is given in Equation 5.

$$W_x = 2x\tan\theta + W_1 \text{ L L L } \xi = \frac{y}{W_x} \quad \text{.....(5)}$$

Thus, for each strip, a different length was used to normalise the data points in the y direction, resulting in normalised distances of the data points falling in the range "0.5 < ξ < +0.5.

The velocity profiles $\frac{u}{U_1}$, for all the strips can thus be plotted on the same graph.

This post processing procedure was performed on the data for all the diffusers and the resulting graphs were similar in appearance to Figure 14. Reverse flow on the unstalled wall near the diffuser entry (values of $\xi \approx 0.5$) was only observed in the 50° diffuser as can be seen from the plot of the $\frac{x}{W_1} = 0.9$ in Figure 14.

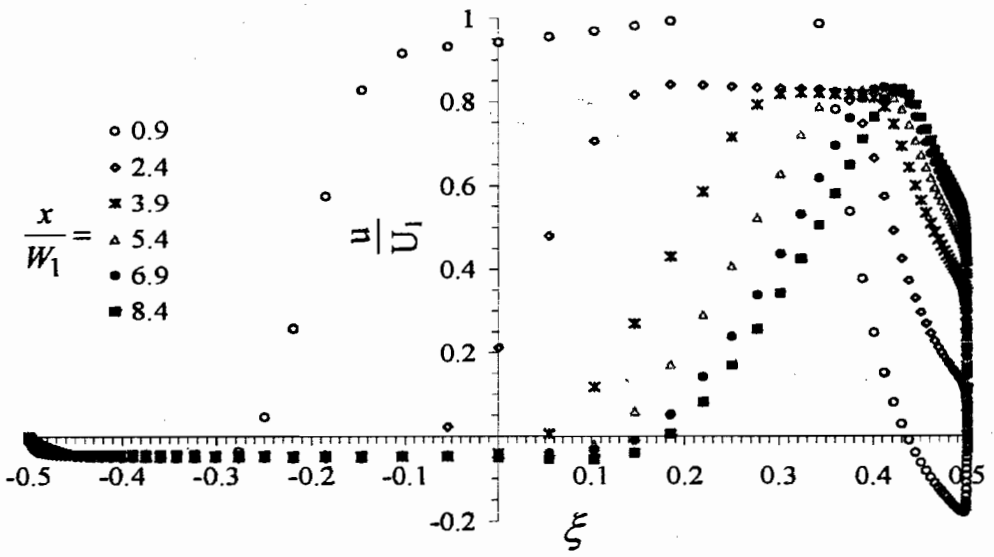

Figure 14: Normalised velocity profiles for the 50 diffuser

From this figure, it is seen that along the left hand portion of each data set corresponding to the different strips, a linear section exists, which intercepts with the abscissa ξ. This intercept gives the location at which the axial velocity u reverses.

At each strip, this intercept is unique and can be denoted as ξ_r. The streamline that is defined by joining ξ_r must then describe the edge of the transition line between regions of unstalled and stalled flow. Six values of ξ_r were obtained for each strip, and eventually for all the angles. Figure 15 shows a plot of these values against the normalised axial distance $\frac{x}{W_1}$.

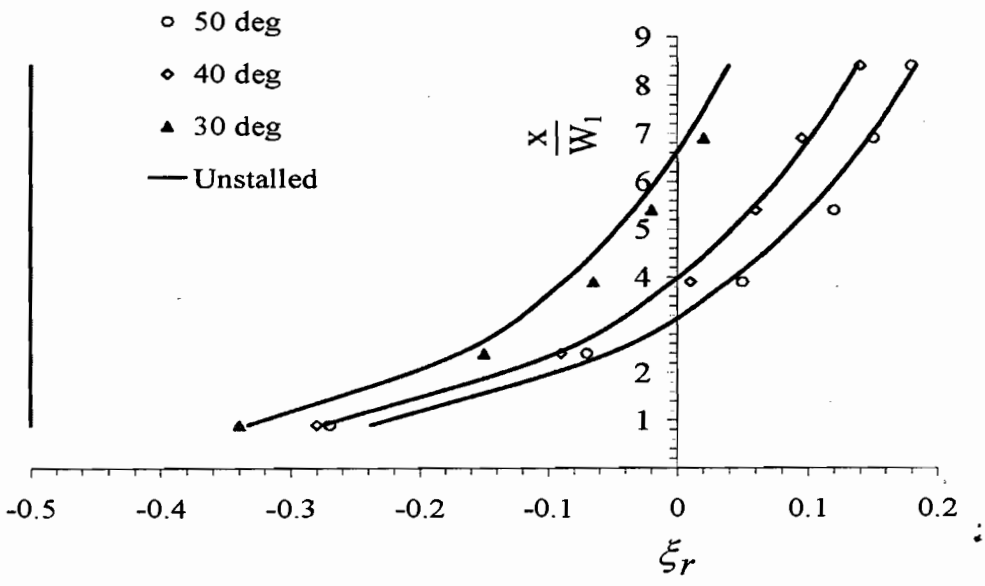

Figure 15: reversal points, ξ_r for diffusers

Inspection of Figure 15 suggests the existence of an exponential relationships between these parameters for $30° \leq 2\theta \leq 50°$, which through curve fitting techniques and computer optimization of the coefficients, were correlated to give Equation 6.

$$\xi_r = \varsigma_1 ln\left(\frac{x}{W_1}\theta^2\right) - \frac{1}{\varsigma_1} ln \frac{1}{\varsigma_2} \quad \text{for } 30°<2\theta<50° \qquad \text{.....(6)}$$

where the coefficients ς_1 and ς_2 are:

$$\varsigma_1 = \frac{1}{7.4 - 0.1\theta}$$
$$\varsigma_2 = \left(0.73\theta^2 + 1323\right)\theta^2 - \left(51.2\theta^2 + 14764\right)\theta + 61291 \qquad \text{.....(7)}$$

The limiting case of ξ_r = "0.5 occurs for unstalled diffusers.

For wide-angled diffusers therefore, if the ratio $\frac{x}{W_1}$ is known, the effective width of flow $0.5 - \xi_r$, as shown in figure 16 can be evaluated.

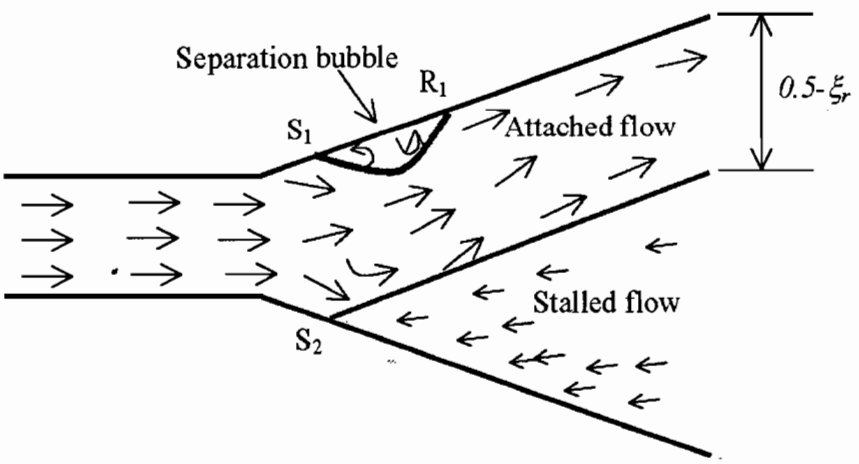

Figure 16: Effective flow-field for wide-angled diffusers

From a boundary layer theory view point, separation of the flow at the wall occurs when the wall shear stress becomes zero. Precisely, at the point of stall $\frac{\partial u}{\partial x} = 0$. The locations of point sS_1 and R_1 in Figure 16 correspond to the points on the curve when = 0 on the unstalled wall. Point S_2 corresponds to the location when = 0 on the stalled wall. With the aid of Equation 6, the effective flow area for wide angled diffusers that are in the fully stalled regime, as represented in figure 16, can be mapped and are summarised in Table 3. The average of the errors between the calculated and measured effective flow areas that results from such mapping is approximately 6%.

Table 3: Mapping of the flow-field

2θ	30°	40°	50°
S_1	0	0	0
R_1	0	0	2.1
S_1	0	0	0
ξ_r at exit	0.09	0.17	0.23
% error in ξ_r	8.00	4.15	6.83

4.0 CONCLUSIONS

In this paper, experimental investigations of separated flows in fully stalled wide-angled diffusers have been carried out. Due to the adverse pressure gradient along the diffuser walls, flow separated from one diverging wall and became attached to the other wall, thus forming a region of steady stall within the diffusers. It was not possible to determine in advance the wall to which the flow would attach. Tests to determine the wall to which the flow remains attached led to the conclusion that the wall of preference was totally random and was probably caused by a slight upstream disturbance that was impossible to detect. However, it was possible to 'switch' the flow from one wall to the other by introducing an inlet disturbance. It was found that once 'switched' to a wall, the flow remained attached to that wall permanently. Experimental results showed that regardless of the wall to which the flow was attached, both the velocity and pressure flow-fields were replicated with discrepancies below 2%.

Although current literature states that for a given geometry, the Reynolds number has little influence on the static pressure recovery, it was found in this study that by increasing the velocity from 10 m/s to 20 m/s, the static pressure recovery for the 30° diffuser increased by 8.31%. However, as the divergence angle was increased, a similar increase in Reynolds number resulted in a higher percentage of pressure recovery. The limited range of Reynolds numbers investigated in this study could not allow a rational correlation between the Reynolds number and the C_{pr} profiles. This range was limited by the physical constraints imposed by the wind tunnel and fan speed. For instance, a change of velocity from 10 m/s to 80 m/s would not change the Reynolds number by even one order of magnitude. The experimental uncertainties in this research were approximately 2%. Within these uncertainties, a reliable data bank contribution has been provided for unvaned fully stalled wide-angled diffusers. The parameters in the data bank include the wall static pressure recovery data, axial and lateral velocity profiles and static pressure profiles.

A simple correlation for determining the effective flow areas for fully stalled diffusers has been proposed. When used together with the separation bubble mapping, separation points on the unstalled and stalled walls, and reattachment point on the unstalled wall can be mapped. Thus, if the effective flow area is predicted in advance, then it is promising that one-dimensional flow theory together with the boundary layer equations can be used to provide useful information in stalled adverse pressure gradient flows.

REFERENCES

Fox R. W. and Kline S. J. (1962). Flow Regime Data and Design Methods for Curved Subsonic Diffusers. *Transactions of the ASME, Journal of Basic Engineering,* **84**, pp 303-312.

Gundogdu M. Y., and Carpinlioglu M. O. (1998). A multi-tube Pressure Probe Calibration Method for Measurements of Mean Flow Parameters in Swirling Flows. *Flow Measurement and Instrumentation,* **9**, pp 243-248.

Hoffmann J. A. (1981). Effects of Free-stream Turbulence on Diffuser Perfromance. *Transactions of the ASME, Journal of Fluids Engineering,* **103,** (3), pp 385-390.

Johnston J. P., and Powars C. A. (1969). Some Effects of Inlet Blockage and Aspect Ratio on Diffuser performance. *Transactions of the ASME, Journal of Basic Engineering,* **91**, pp 551-553.

Kaiser K. F. and McDonald A. T. (1980). Effect of Wake-type Nonuniform Inlet Velocity Profiles on First Appreciable Stall in Plane-wall Diffusers. *Transactions of the ASME, Journal of Fluids Engineering,* **102**(3), pp 283-289.

K. Kibicho (2006). Flow-Field Structure in Wide-Angled Diffusers. PhD thesis, University of Cape Town, South Africa.

Kibicho P. K. and Sayers A. T. (2005). Velocity and Static Pressure Profiles in Wide Angled Two-dimensional Stalled Diffuser Flows, Fluid Structure Interaction 2005, La Coruna, Spain.

Kibicho P. K., Suzuki T. and Waka R. (2001). Study on Subsonic Two-dimensional Diffuser Flows. *Journal of Agriculture Science and Technology,* **3**(2), pp 68 - 83.

Kline S. J. (1959). On the Nature of Stall. *Transactions of the ASME, Journal of Basic Engineering,* **81**, pp 305-321.

Kline S. J., Abbort D. E. and Fox R. W. (1959). Optimum Design of Straight-walled Diffusers. *Transactions of the ASME, Journal of Basic Engineering,* **81**, pp 321-331.

McMillan O. J. and Johnston J. P. (1973). Performance of Low-aspect Ratio Diffusers withFull Developed Turbulent Inlet Flows-some Experimetal Results. *Transactions of the ASME, Journal of Fluids Engineering,* **95**(3), pp 385-392.

Norbury J. F. (1959). Some Measurements of Boundary-layer Growth in a Two-dimensional Diffuser. *Transactions of the ASME, Journal of Basic Engineering,* **81**, pp 285-296.

Reneau L. R., Johnston J. P. and Kline S. J. (1967). Performance and Design of Straight, Two-dimensional Diffusers. *Transactions of the ASME, Journal of Basic Engineering,* **89**(1), pp 141-150.

Rhagava A. K., Kumar K. L., Malhotra R. C. and Agrawal D. P. (1979). A Probe for the Measurement of Velocity Field. *Transactions of the ASME, Journal of Fluids Engineering,* **11**(1), pp143-146.

Runstadler P. W. and Dean R. C. (1969). Straight Channel Diffuser Performance at High inlet MachNumbers. *Transactions of the ASME, Journal of Basic Engineering,* **91**, pp 397-422.

Sagi C. J., and Johnston J. P. (1967). The design and performance of two-dimensional, curved diffuserspart i- exposition of method. *Transactions of the ASME, Journal of Basic Engineering,* **89**, 715-731.

Wolf S. and Johnston J. P. (1969). Effects of Nonuniform Inlet Velocity Profiles on Flow Regimes and Performance in Two-dimensional Diffusers. *Transactions of the ASME, Journal of Basic Engineering,* **91**(3), pp 462-474.

Yajnik K. S. and Gupta R. P. (1973). A new probe for measurement of velocity and flow direction in separated flows. *Journal of Physics, Series E, Science Instrumentation,* **6**, pp 82-86.

APPENDIX: DATA BANK CONTRIBUTION

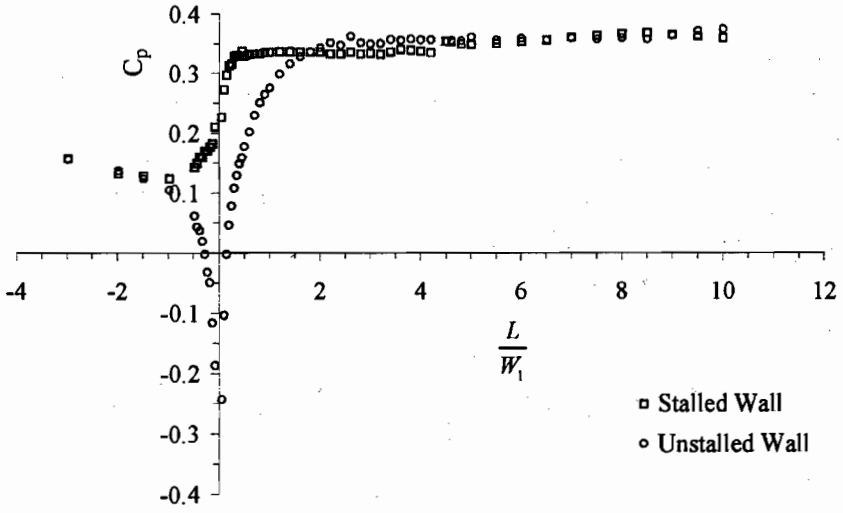

Figure 17: Coefficient of static pressure for the 30 ° diffuser

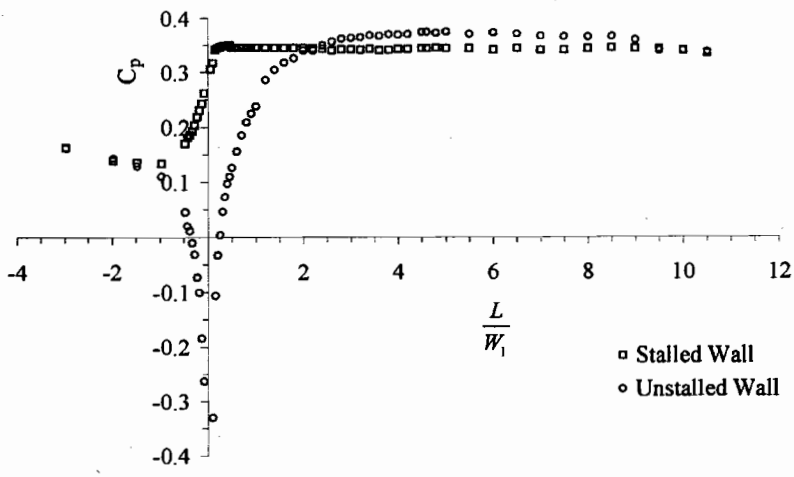

Figure 18: Coefficient of static pressure for the 40 ° diffuser

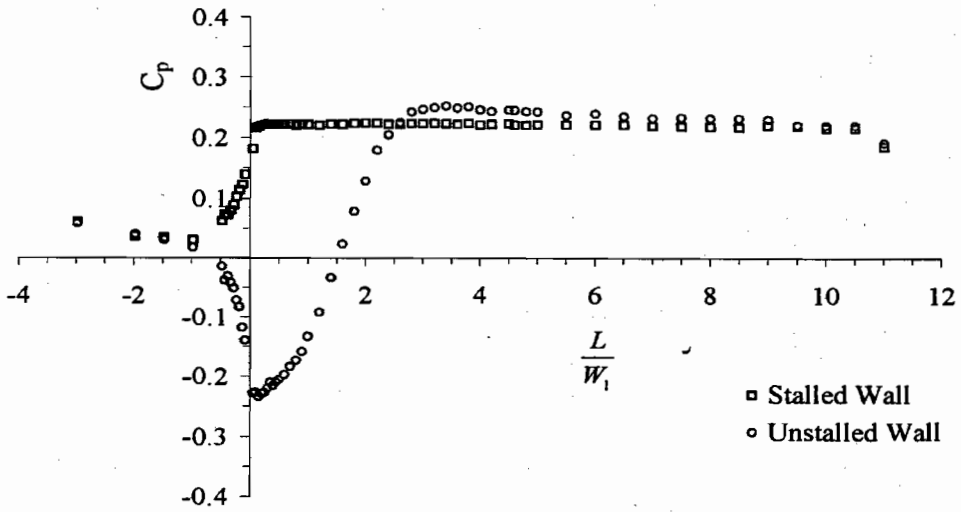

Figure 19: Coefficient of static pressure for the 50° diffuser

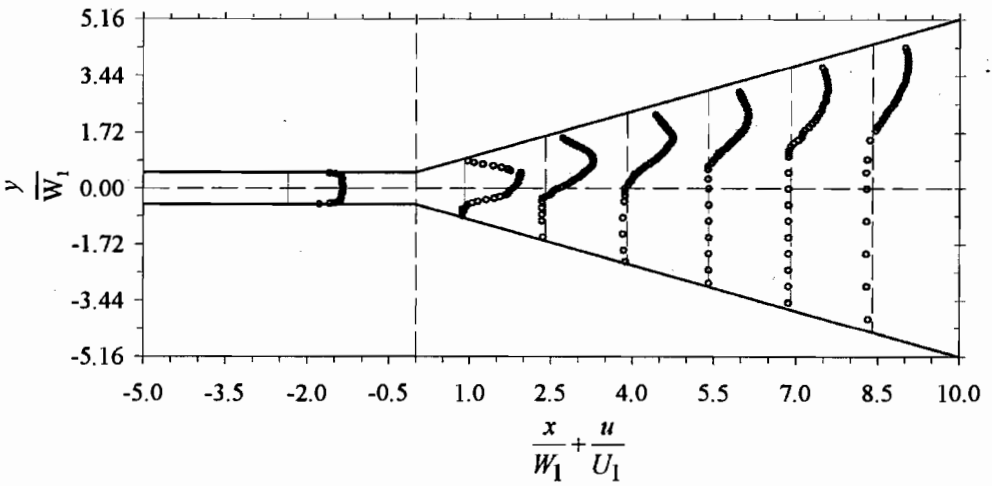

Figure 20: Axial velocity profiles for the 50° diffuser

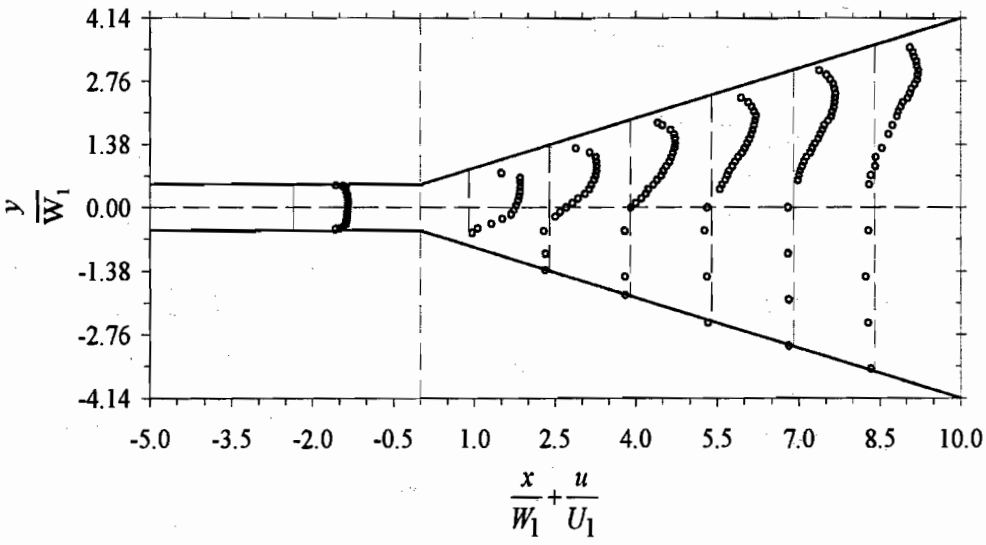

Figure 21: Axial velocity profiles for the 40 ° diffuser